REVIEW AND COMPARISON OF SIMULATION CODES MODELING ELECTRON-CLOUD BUILD UP AND INSTABILITIES

E. Benedetto, F. Ruggiero, D. Schulte, F. Zimmermann, CERN; M. Blaskiewicz, L. Wang, BNL;
G. Bellodi, RAL/ASTeC; G. Rumolo, GSI; K. Ohmi, S.-S. Win, KEK; M. Furman, LBNL;
Y. Cai, M. Pivi, SLAC; V. Decyk, W. Mori, UCLA; A.F. Ghalam, T. Katsouleas, USC

Abstract

Several computer codes written at various laboratories are employed for modeling the generation and the consequences of an electron cloud. We review several of these programs, which simulate either the build up of an electron cloud or the instabilities it produces, and we compare simulation results for identical, or similar, input parameters.

INTRODUCTION

At many accelerator laboratories computer codes have been developed in the attempt to predict electron-cloud effects at operating or future machines. The underlying assumptions and models of the various codes are somewhat different, and so likely are their predictions, if applied to the same problem. To understand the impact of various model assumptions, an inter-laboratory code-comparison effort was launched after ECLOUD'02 and revived at ECLOUD'04 [1].

BUILD-UP SIMULATIONS

The reference case for the build-up simulations is described in Table 1. The parameters resemble those of the LHC proton beam. Primary 'seed' electrons are created at a rate of 0.001 per proton per meter on the chamber wall. The quantity of interest is the electron line density as a function of time. Results are available from the codes CSEC (M.B.), ECLOUD (G.B., G.R., D.S., F.Z.), EPI and PEI (K.O.), POSINST (M.P., M.F.), and CLOUDLAND (L.W.). They are shown in Fig. 1. The electron line density at saturation and the number of bunches until saturation are summarized in Table 2. The simulated saturation densities differ by a factor 3–4, the build-up time by even more.

Table 1: Parameters for build-up simulations

variable	symbol	value
bunch population	N_b	1×10^{11}
number of bunches	n_b	20
bunch spacing	L_{sep}	7.48 m
bunch profile		Gaussian
rms bunch length	σ_z	7.7 cm
rms transv. size	$\sigma_{x,y}$	300 μm
round chamber radius	b	2 cm
magnetic field	B	none
max. secondary yield	$\delta^*_{\max}$	1.6
energy at max. yield	$\epsilon^*_{\max}$	250 eV
elastic refl. of low-energy e$^-$		yes, variable

The differences are largely explained by the different modeling of secondary emission, in particular by differences in the probability of reflection of low-energy electrons, and in the energy distribution of the secondary electrons. The total secondary emission yield $\delta(E, \theta)$, which depends on the energy of the primary electron, E, and its angle of incidence on the wall, θ, is considered as consisting of one, two or three components, namely true secondaries, elastically reflected electrons, and rediffused ones:

$$\delta(E, \theta) = \delta_{\text{true}}(E, \theta) + \delta_{\text{el}}(E, \theta) + \delta_{\text{redif}}(E, \theta) . \quad (1)$$

Following [2], the yield for true secondaries is modeled by

$$\delta_{\text{true}}(E, \theta) = \delta_{\max} \frac{s(E/\epsilon_{\max})}{s - 1 + (E/\epsilon_{\max})^s} , \quad (2)$$

where $s \approx 1.35$ for LHC copper samples [3], $\delta_{\max} = \delta^*_{\max} \exp(0.5(1 - \cos \theta))$ [4, 5], $\epsilon_{\max} = \epsilon^*_{\max}(1 + 0.7(1 - \cos \theta))$ [2]. The present version of ECLOUD assumes that low-energetic electrons are reflected from the wall with a probability of 1 in the limit of zero energy, using the parametrization (with $E_0 \approx 150$ eV) [6]:

$$\delta_{\text{el}} = \left((\sqrt{E} - \sqrt{E + E_0})/(\sqrt{E} + \sqrt{E + E_0}) \right)^2 , \quad (3)$$

which is independent of θ. The simulations with PEI and EPI consider a low-energy reflection probability $\delta_{\text{el}}(E)$ parameterized by an exponential fall-off,

$$\delta_{\text{el}}(E) = \exp(-E/E_w) \quad (4)$$

with width $E_w = 10$ eV. The energy distribution of the secondaries is centered at 5 or 10 eV, with a spread of ± 5 eV in either case. The EPI simulations show that the electron density differs by a factor of 3, depending on the central value of the secondary electron energy. The POSINST simulation in Fig. 1 refers to an elastic reflection [7]

$$\delta_{\text{el}} = \left(\hat{P}_{\text{el}} - P_e(\infty) \right) e^{-(E/E_w)^p/p} + P_e(\infty) , \quad (5)$$

with $\hat{P}_{\text{el}} \simeq +0.0408$, $P_e(\infty) \simeq 6.28 \times 10^{-4}$, $E_w = 120$ eV and $p = 0.61$, approximating an old ECLOUD model [5]

$$\delta_{\text{el}} = f/(1 - f)\delta_{\text{true}} \quad (6)$$

where $\ln f = A_0 + A_1 \ln (E + E_0) + A_2 \ln (E + E_0))^2 + A_3 \left(\ln(E + E_0) \right)^3$, with, at energies E below 300 eV, $A_0 \approx 20.7$, $A_1 \approx -7.07$, $A_2 \approx 0.48$, $A_3 \approx 0$, and $E_0 \approx 56.9$. For this example, the probability of elastic reflection approaches $\delta_{\text{el}}(0) \approx 0.4$ at zero incident electron energy E. Without elastic reflection the saturation density is 3 times lower, whereas it is 50% larger if the reflection probability is modeled by an exponential fall-off

$$\delta_{\text{el}}(E) = R_0 \exp(-E/E_w) \quad (7)$$

with width $E_w = 70$ eV and $R_0 = \delta_{\text{el}}(0) \approx 0.5$.

The saturation density found by CSEC with $\delta_{\text{el}}(0) = 0.5$ is 2.5 times higher than the POSINST result based on (5) in

the figure, and still 1.5–2 times higher than the POSINST result obtained using (7) (not shown).

There are other differences between the codes, e.g., in the secondary energy distribution. For example, the ECLOUD code considers an emitted electron energy distribution for true secondaries of the form

$$(dN_s)/(dE_s) \propto \exp\left[-0.5\left(\ln\left(E_s/E_{s0}\right)\right)^2\right] \quad (8)$$

with $E_{s0} \approx 1.8$ eV from Ref. [5], which goes to zero at zero energy E_s. Other codes employ uniform, Gaussian or Lorentzian distributions. The result from EPI in Fig. 1 illustrates that the choice of secondary energy distribution can greatly affect the simulated electron build up.
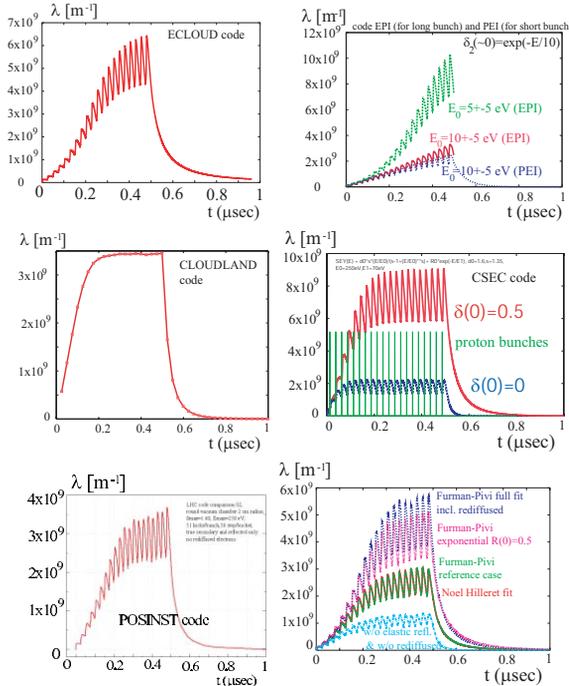

Figure 1: Results of build-up simulations for the example case by various codes: ECLOUD with (3) (top left), EPI and PEI (top right), CLOUDLAND (centre left), CSEC (centre right), POSINST (bottom left), ECLOUD using the four parametrizations of Fig. 2 [same colors] and a fifth case without elastic reflection [cyan] (bottom right).

Table 2: Results of build-up simulations

code	final e^- line density [m^{-1}]	no bunches to saturation
ECLOUD	5×10^9	17
EPI	$2.5 - 9 \times 10^9$	≥ 20
PEI	2×10^9	≥ 20
CLOUDLAND	3.4×10^9	8
CSEC	$2 - 3 \times 10^9$	3–8
POSINST	3×10^9	13

Yet another representation of the secondary emission in simulations for ISIS and PSR [8] approximates the probabilistic model routinely used in POSINST [9]. Here, elastically reflected electrons, rediffused and true secondaries are distinguished. Electrons are assigned to either category

according to the relative ratio of $\delta_{\rm el}$, $\delta_{\rm redif}$ and $\delta_{\rm true}$ over the total yield δ at the corresponding E and θ. The functional forms of these components are

$$\delta_{\rm el} = \left[0.07 + 0.336 e^{-(E/100)}\right]\left[1 + 0.26(1 - \cos^2\theta)\right],$$

$$\delta_{\rm redif} = 0.578(1 - e^{-(E/40)})\left[1 + 0.26(1 - \cos^2\theta)\right],$$

$$\delta_{\rm true} = \frac{1.722 E/\epsilon_{\rm max}}{0.813 + (E/\epsilon_{\rm max})^{1.813}}\left[1 + 0.66(1 - \cos^{0.8}\theta)\right] \quad (9)$$

where E is in units of eV, and all coefficients have been scaled so that $\hat{\delta}_t$=1.6 at $\hat{E}_t$=260 eV (for the case of stainless steel in [9]). Reflected secondary electrons are assigned the same angular distribution and the same energy as the incident electron (with a small Gaussian smearing). The energy of the rediffused electrons is given by: $E = E_0 r^{0.7}$ where r is a uniformly distributed random number in [0,1], while the energy of true secondaries follows a Gaussian distribution centered at 10 eV with σ=5eV.

Figure 2 shows four different parametrizations of the secondary emission yield, that were programmed in ECLOUD and POSINST for the purpose of comparison [8, 7]. The bottom right picture in Fig. 1 presents results from a modified version of ECLOUD for the same four parametrizations of elastic reflection and a fifth one with true secondaries only. For the identical model of secondary emission (green curve) the agreement of the modified ECLOUD code with the POSINST result in Fig. 1 (left bottom) is at the 20% level. However, there is nearly a factor two difference, when either considering the full model, including rediffused (dark blue curve) or the alternative representation (7) with a higher proportion of elastically reflected electrons at low energy (the purple curve). Similar differences were seen when comparing different secondary-emission models within POSINST [7].
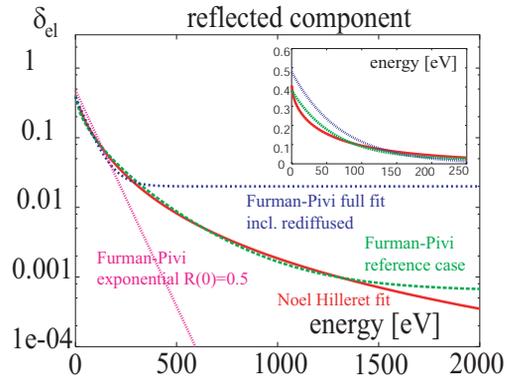

Figure 2: Different parametrizations of elastic reflection: formula (6) [5] [red], expression (5) [green], alternative (7) with $\delta_{\rm el0} \approx 0.5$ [purple], and parametrization (9) which approximates [9], and includes a rediffused component [blue]. The inset shows a detail of the plot at low energy on a normal non-logarithmic scale.

Figure 3 displays energy distibutions of secondaries for four different incident energies, computed using the approximation (9) and one based on (6) [8]. Figure 4 compares build-up simulations with these two models for ISIS and the PSR. The PSR case is sensitive to the model.
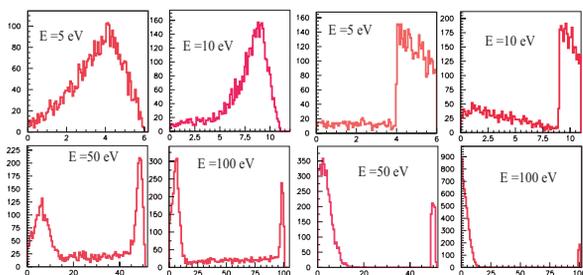
Figure 3: Secondary-energy spectra for different incident energies E; left: for POSINST model (9) [9], right: for a model based on expression (6) [5].
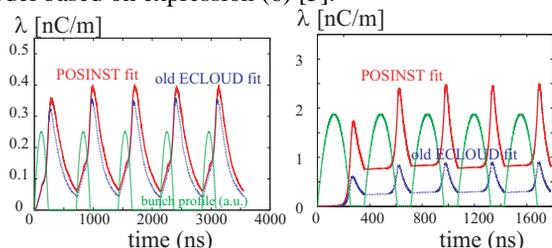

Figure 4: Comparison of build-up simulations with the ECLOUD for ISIS (left) and PSR, using either the POSINST model (9) [9], or the expression (6) [5] for the secondary emission.

INSTABILITY SIMULATIONS

The reference case for the single-bunch instability simulations is described in Table 3. The parameters resemble those of the LHC proton beam in the SPS. The quantity of interest is the evolution of the horizontal and vertical emittance as a function of time. Results are available from the codes HEADTAIL (E.B., G.R.), PEHTS (K.O.) and QUICKPIC (A.G., T.K.) [10]. They are presented in Fig. 5 and initial emittance growth rates are summarized in Table 4. The last picture illustrates the sensitivity to the number of interaction points and to the boundary conditions. As the number of IPs increases the results of the discrete codes PEHTS [11] and HEADTAIL [12] seem to approach that of the continuous code QUICKPIC [10].

CONCLUSION AND OUTLOOK

Build-up and instability simulation codes can produce results that vary by factors 3–100. The differences reflect a strong sensitivity to modeling details. Updated information at *http://wwwslap.cern.ch/collective/ecloud02/ecsim* . Work supported in part by US-LARP, EU via CARE, U.S. DOE (Contract No. DE-AC03-76SF00098), and NERSC.

REFERENCES

[1] ECLOUD'02, Geneva, 15-18 April, 2002, Workhop Proceedings, CERN-2002-001; web site *http://wwwslap.cern.ch/collective/ecloud02*'. ECLOUD'04, Napa, April 19–23, 2004; web site *http://icfa-ecloud04.web.cern.ch/icfa-ecloud04/.*

[2] M. Furman et al., MBI 97 Tsukuba, KEK 97-17 (1997).

[3] V. Baglin et al., LHC Project Report 472 (2002).

[4] R. Kirby, F. King, NIM A469, 1–12 (2001).

Table 3: Parameters for instability simulations with smooth focusing, no synchrotron motion, a Gaussian bunch profile, either open or conducting boundaries condutions in the field calculation, a variable number of beam-electron interaction points (IPs), no magnetic field, zero chromaticity and zero energy spread

variable	symbol	value
bunch population	N_b	1×10^{11}
electron density	ρ_e	10^{12} m^{-3}
round chamber radius	b	2 cm
beta function	$\beta_{x,y}$	100 m
beam energy	E_b	20 GeV
ring curcimference	C	5 km
betatron tunes	$Q_{x,y}$	26.19, 26.24
rms bunch length	σ_z	30 cm
rms transv. size	$\sigma_{x,y}$	2 mm

Table 4: Emittance growth in instability simulations

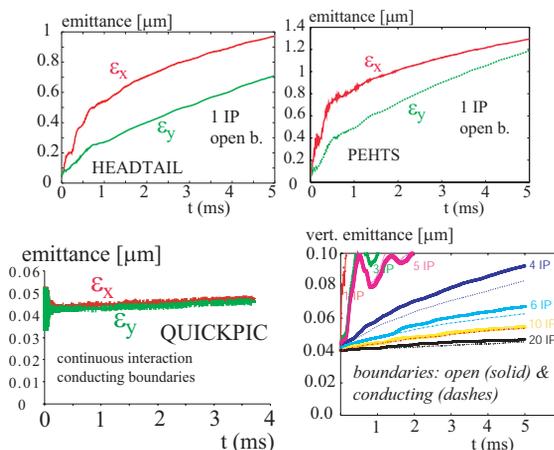| code	horizontal [%/ms]	vertical [%/ms]
HEADTAIL 1, 20 IPs	1250, 3	375, 3
PEHTS 1, 20 IPs	2000, 10	1000, 10
QUICKPIC	2	2

Figure 5: Results of instability simulations for the example case by various codes: HEADTAIL with 1 IP (top left), PEHTS (top right), QUICKPIC (bottom left), and HEADTAIL with various numbers of IPs for both open and conducting boundaries .

[5] B. Henrist, N. Hilleret, et al., in [1].

[6] C. Herring et al., Rev. Mod. Phys. 21, 2, 187 (1949); R. Cimino et al., CERN-AB-2004-012-ABP.

[7] M. Furman, M. Pivi, "LHC Electron Cloud Simulation Code Comparison," 5. September 2002.

[8] G. Bellodi, unpublished (2004).

[9] M. Pivi and M. Furman, PRST-AB 5, 124404 (2002).

[10] G. Rumolo, A.Z. Ghalam et al., PRST-AB 6, 081002 (2003).

[11] K. Ohmi, "Single Bunch Electron Cloud Instability for a Round Beam (Memo)," 19. Nov. 2002.

[12] E. Benedetto et al., "Transverse Monopole Instability Driven by an Electron Cloud?," PAC 2003 Portland.